



Compositional-dependent properties of Pr³⁺-doped multicomponent fluoro-phosphate glasses for visible applications: a photoluminescence study

S. Babu¹, P. Rajput², and Y. C. Ratnakaram^{1,*}

¹Department of Physics, Sri Venkateswara University, Tirupati, A.P 517 502, India

²Atomic & Molecular Physics Division, Bhabha Atomic Research Centre, Trombay, Mumbai 400085, India

Received: 26 February 2016

Accepted: 17 May 2016

Published online:

31 May 2016

© Springer Science+Business Media New York 2016

ABSTRACT

Five fluoro-phosphate (FP) glasses of different compositions, 49.5P₂O₅–10AlF₃–10BaF₂–10SrF₂–10PbO–10M (M = Li₂O, Na₂O, K₂O, ZnO, and Bi₂O₃), doped with 0.5 mol% praseodymium were prepared by melt quenching technique. For these glass matrices, structural, thermal, dielectric, electrical, and optical properties have been studied. The structures are characterized by XRD, Fourier transform infrared, Raman spectroscopy, and solid-state ³¹P and ²⁷Al magic angle spinning nuclear magnetic resonance techniques. The chemical and electronic states of these glass materials are characterized by X-ray photoelectron spectroscopy. The thermal stability for the host glass matrix is estimated from differential scanning calorimetry technique. From the impedance spectroscopy, various parameters, viz. electrical conductivity, dielectric constant (ϵ'), and dielectric losses ($\tan \delta$), at various frequencies and temperatures have been measured. X-ray absorption near-edge spectroscopy was used to study the electronic structure of praseodymium in the host glass matrices. By analyzing the absorption spectra with Judd–Ofelt theory, three intensity parameters (Ω_{λ} , $\lambda = 2, 4, 6$) are obtained. In turn, these parameters are used to calculate radiative properties such as emission probabilities (A_R), radiative lifetimes (τ_R), and integrated absorption cross sections (Σ) of different Pr³⁺ transitions. Luminescence parameters such as stimulated emission cross sections (σ_p) and branching ratios (β_{exp}) have been studied through photoluminescence spectra. Further, decay time constants are estimated from the decay profiles of Pr³⁺-doped different FP glasses.

Address correspondence to E-mail: ratnakaramsvu@gmail.com

Introduction

Glass is very flexible and a good host for rare-earth (RE) ions; it provides high optical transparency and good RE ion solubility, and it can be transmitted to almost any shape or size. Glasses doped with RE ions have been extensively investigated due to their emission ranging from visible to near-infrared (IR) regions [1].

Phosphates are very diverse class of compounds whose properties cover all aspects of material science and physics. Among different types of glasses, renewed interest for the selection of fluoro-phosphate (FP) glass is due to its low melting point, UV to IR region transparency, low refractive index, low phonon energy, and high emission cross sections [2]. The origin of these properties has been strongly related to the local order around phosphorous atoms. The coordination geometry of phosphorous atoms is decided by the glass composition and the nature of the glassy network modifiers. In order to dope high level of RE concentration in the host glass matrix, glass modifiers are added which breaks the bridging anion bonds, thus increasing the non-bridging bonds. Alkali and alkaline earth oxides act as glass modifiers in the phosphate network former. RE ions are engaged in the vicinity of non-bridging oxygen bonds. The main disadvantage of these glasses is poor chemical resistivity. In this context, fluorine content is added in the form of a variety of metal fluorides. Hence, FP glasses contain the properties of both fluoride and phosphate glasses [3].

In order to interpret the best property–performance correlation and for improving optical properties, a better knowledge on the structure of FP glass is important. The structure of phosphate compounds is rather complex with various sites available for occupation by divalent/trivalent cations. To gain further approaching in the structure of host matrices, solid-state nuclear magnetic resonance (NMR) and X-ray photoelectron spectroscopy (XPS) techniques are useful. As NMR is an element-selective method sensitive to the local environments, well suited for distinguishing different local environments present in glassy material. The type of phosphate and aluminate structural units are known by NMR spectra [4].

Among the different RE ions, Pr^{3+} had been studied extensively for sensor, special band amplification and IR lasers. Materials doped with Pr^{3+} were investigated for optical imaging due to the Pr^{3+}

energy level scheme which contains several metastable multiplets ($^3\text{P}_0$, $^1\text{D}_2$ and $^1\text{G}_4$) [5]. Recently, Zhang et al. [6] studied luminescence and Judd–Ofelt (J–O) analysis of the Pr^{3+} -doped fluorotellurite glass. Anjaiah et al. [7] reported luminescence properties of Pr^{3+} doped Li_2O – MO – B_2O_3 glasses. Burtan-Gwizdala et al. [8] investigated the influence of Pr^{3+} content on the luminescence and optical behavior of TeO_2 – WO_3 – PbO – Lu_2O_3 glass.

The present work is mainly focuses on optimization of host FP glass composition which exhibit better optical, radiative, and luminescence properties. Structural modifications imposed by the variation of host glass composition were studied by Fourier transform infrared (FTIR), Raman, solid-state NMR, and XPS. Thermal nature is obtained from differential scanning calorimetry (DSC) thermal profiles. Dielectric and electrical behavior of glassy material was studied by impedance spectroscopy. To confirm the oxidation state of praseodymium in the glass system, X-ray absorption near-edge spectroscopy (XANES) was undertaken. Further, this study consists of optical absorption, fluorescence, and emission lifetimes measurements. In order to predict radiative properties and to study the radiative transition probabilities (A_R), radiative lifetimes (τ_R), branching ratios (β_R), absorption cross sections (Σ), and peak emission cross sections (σ_p), J–O theory has been applied to the absorption spectra.

Experimental

Different FP glasses were prepared from raw materials with 99.9 % purity phosphorous pentoxide (P_2O_5), aluminum fluoride (AlF_3), barium fluoride (BaF_2), strontium fluoride (SrF_2), lead oxide (PbO), lithium carbonate (Li_2CO_3), sodium carbonate (Na_2CO_3), potassium carbonate (K_2CO_3), zinc oxide (ZnO), bismuth oxide (Bi_2O_3), and praseodymium oxide (Pr_6O_{11}). Final glass compositions of the prepared glass samples are labeled as follows (in mol%):

1. Li: 49.5 P_2O_5 –10 AlF_3 –10 BaF_2 –10 SrF_2 –10 PbO –10 Li_2O –0.5 Pr_6O_{11} ,
2. Na: 49.5 P_2O_5 –10 AlF_3 –10 BaF_2 –10 SrF_2 –10 PbO –10 Na_2O –0.5 Pr_6O_{11} ,
3. K: 49.5 P_2O_5 –10 AlF_3 –10 BaF_2 –10 SrF_2 –10 PbO –10 K_2O –0.5 Pr_6O_{11} ,
4. Zn: 49.5 P_2O_5 –10 AlF_3 –10 BaF_2 –10 SrF_2 –10 PbO –10 ZnO –0.5 Pr_6O_{11} , and

5. Bi: 49.5P₂O₅–10AlF₃–10BaF₂–10SrF₂–10PbO–10Bi₂O₃–0.5Pr₆O₁₁.

The appropriate mixtures of these compounds were thoroughly crushed in an agate mortar in order to have proper mixing and homogeneity. The homogeneously mixed chemicals were taken in porcelain crucible and melted at 1100–1150 °C for 45 min in an electric furnace depending upon chemical composition. The melt was cast on a pre-heated brass plate and pressed by another brass plate. Then the glasses were obtained. The glass samples were subsequently annealed in order to eliminate internal mechanical stresses.

The density was measured according to Archimedes' principle using clean water as an immersion liquid. The refractive indices of the glasses were measured using an Abbe refractometer. These values were found in the range of 1.650–1.652 for all glass matrices studied. The amorphous nature of host glass matrices were confirmed through the X-ray diffraction (XRD) studies using SIEFERT diffractometer employing Cu K α radiation at 40 kV applied voltage and 30 mA anode current with a Si detector. The range of diffractometer was from 5° to 70° with step size of 0.02°. SEM images were recorded using Carl Zeiss EVO-MA15 scanning electron microscope. FTIR spectra were recorded using a model of Perkin Elmer spectrum One FT-IR spectrophotometer. Raman spectra were obtained in back-scattering geometry with 514 nm line of Ar⁺ laser as an excitation source at power of 10 mW. The spectral slit width was 1 mm, and accumulation number was 50 s. Solid-state NMR spectra were recorded to further study the structural evolution of prepared glasses using JEOL DELTA 2 NMR at 9.4 T with a 4-mm probe. The acquisition time was 18 ms and pulse width was 2.9 μ s. The spinning speed was 10 kHz. XPS spectra were recorded using a Thermo Scientific K-Alpha. Thermal profiles were recorded using DSC on a Seiko SII DSC 6220 with a Seiko SII EXSTAR 6000PC Station under nitrogen flow, at a scanning rate of 10 °C min⁻¹. Dielectric and electrical measurement were done using HIOKI 3532-50 LCR HiTESTER (Japan) model. XANES measurements of glass samples at L3 edge were carried out in fluorescence mode at the Scanning EXAFS Beamline (BL-9) at the INDUS-2 Synchrotron Source (2.5 GeV, 100 mA) at the Raja Ramanna Centre for Advanced Technology (RRCAT), Indore, India. The beamline uses a double-

crystal monochromator (DCM) which works in the photon energy range of 4–25 keV with a resolution of 10⁴ at 10 keV. A 1.5-m horizontal pre-mirror with meridional cylindrical curvature was used prior to the DCM for collimation of the beam and higher harmonic rejection. The second crystal of the DCM was a sagittal cylinder with radius of curvature in the range 1.28–12.91 m which provides horizontal focusing to the beam. For measurements in the fluorescence mode, the sample was placed at 45° to the incident X-ray beam, and the fluorescence signal (I_f) was detected using a Si drift detector placed at 90° to the incident X-ray beam. An ionization chamber detector is used prior to the sample to measure the incident X-ray flux (I_0), and the absorbance of the sample ($\mu = I_f/I_0$) was obtained as a function of energy by scanning the monochromator over the specified energy range. The optical absorption spectral measurements were collected using a Varian Cary 5000 spectrophotometer in UV–Vis region with 0.01 nm steps and in NIR region with 0.04 nm steps, with the resolution of <0.05 and <0.2 in the UV–Vis and NIR regions, respectively. The excitation, photoluminescence spectra, and decay curves of Pr³⁺-doped glass samples were recorded using Jobin–Yvon Fluorolog-3 spectrofluorometer (Horiba FL3-22iHR320). All these measurements were conducted at room temperature.

Results and discussion

XRD and SEM analysis

XRD scans were performed for all host glasses. The XRD pattern of lithium FP glass is shown in Fig. 1. The inset of Fig. 1 shows the SEM image of lithium FP glass without diffraction peaks, indicating amorphous nature. Similar profile was obtained for other FP glass samples. So, we did not show for other glass matrices. These glasses were found homogeneous and without any particle aggregates indicating amorphous nature of glasses through SEM analysis.

Vibrational spectroscopy

The chemical structure of the prepared host FP glass samples was analyzed using FTIR in the range 650–3800 cm⁻¹, and the spectra are shown in Fig. 2. The absence of sharp like bands in the FTIR spectra

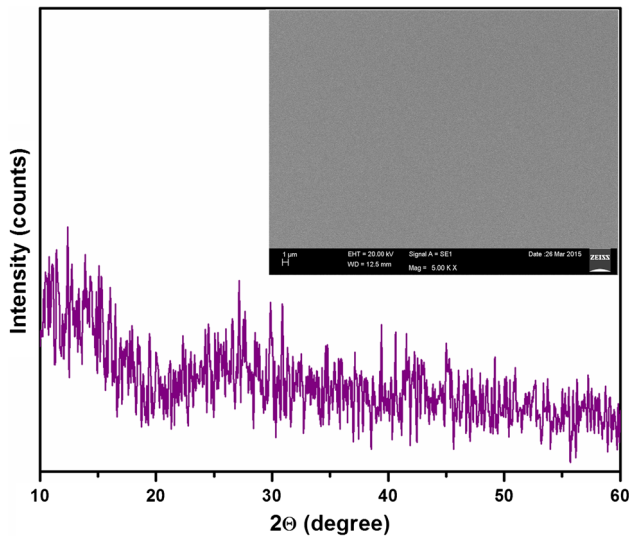


Figure 1 XRD pattern with SEM image of lithium FP host glass matrix.

was an indicative disorder in the FP glass units. The band at 730 cm^{-1} was attributed to symmetric stretching vibrations of P–O–P bridging oxygen groups [9]. The band at $\sim 900\text{ cm}^{-1}$ was related to asymmetric stretching vibration of P–O–P and P–F groups [10]. Asymmetric stretching vibration mode of P–O–P non-bridging oxygen groups indicated the band in the range $1065\text{--}1085\text{ cm}^{-1}$. The band at 1240 cm^{-1} was related to asymmetric P=O vibrations in all the glass matrices except in bismuth FP glass. The band at 3730 cm^{-1} was attributed to symmetric stretching vibration of OH groups [11].

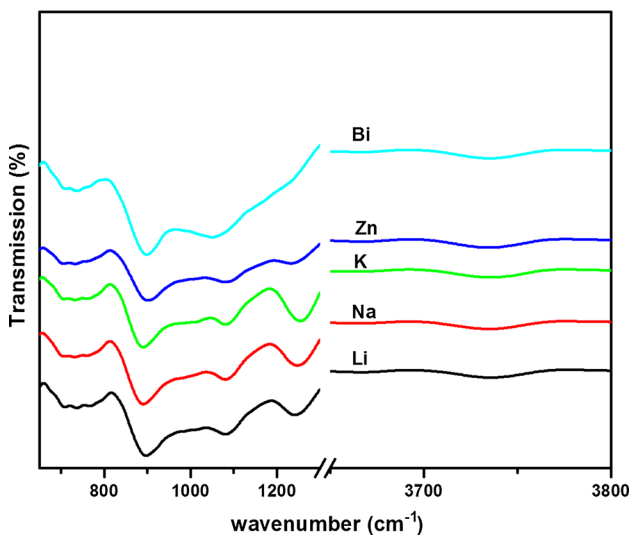


Figure 2 FTIR transmittance spectra of different FP host glasses.

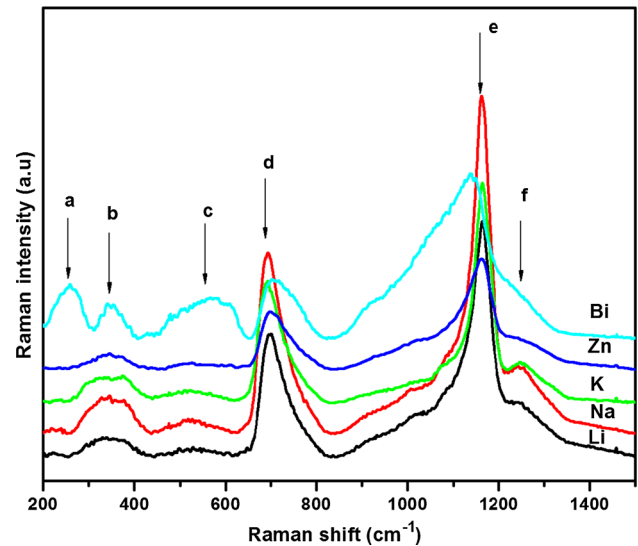


Figure 3 Raman spectra of different FP host glasses.

Raman spectroscopy

The Raman spectra for the different host FP glasses are shown in Fig. 3. Summary of Raman bands is described in Table 1. The band at 257 cm^{-1} belongs to symmetric stretching vibrations of Bi–O bonds in BiO_3 and BiO_6 units [12]. The appearance of this band in bismuth FP glass suggests the structural coordination changes in the phosphate network. Raman modes observed at 330 cm^{-1} associated to the network glass structure and rocking motion of PO_4 tetrahedra [13]. The presence of this band indicates that different modifier oxides act as network modifiers in the vicinity of phosphate glass structure. The band at $525\text{--}570\text{ cm}^{-1}$ was associated to deformation mode of P–F vibrations [14] and the band at 696 cm^{-1} to symmetric stretching mode of P–O–P linkages. The strong band at $1130\text{--}1160\text{ cm}^{-1}$ was associated with symmetric stretching of O–P–O non-bridging oxygen atoms of phosphate group, and the band at $1240\text{--}1250\text{ cm}^{-1}$ was related to symmetric stretching of P=O terminal oxygen group [15]. In the case of bismuth FP glass, this band was not observed. The phonon energy of the host could be defined as the highest vibrational energy measured from the Raman spectrum, and it was found to be $1130\text{--}1160\text{ cm}^{-1}$ for FP glasses.

Magic angle spin nuclear magnetic resonance (MAS NMR) analysis

The ^{31}P and ^{27}Al MAS NMR data were recorded for all the prepared host FP glasses and are shown in Fig. 4a, b, respectively. The MAS NMR spectrum of

Table 1 Observed Raman shifts with corresponding band assignments

Symbol	Raman shift (cm ⁻¹)	Band assignments
a	257	Bi–O bonds in BiO ₃ and BiO ₆ units
b	330	Network modifying groups
c	525–570	Deformation mode of P–F vibrations
d	696	P–O–P bridging oxygens
e	1130–1160	O–P–O non-bridging oxygens
f	1240–1250	P=O terminal oxygens

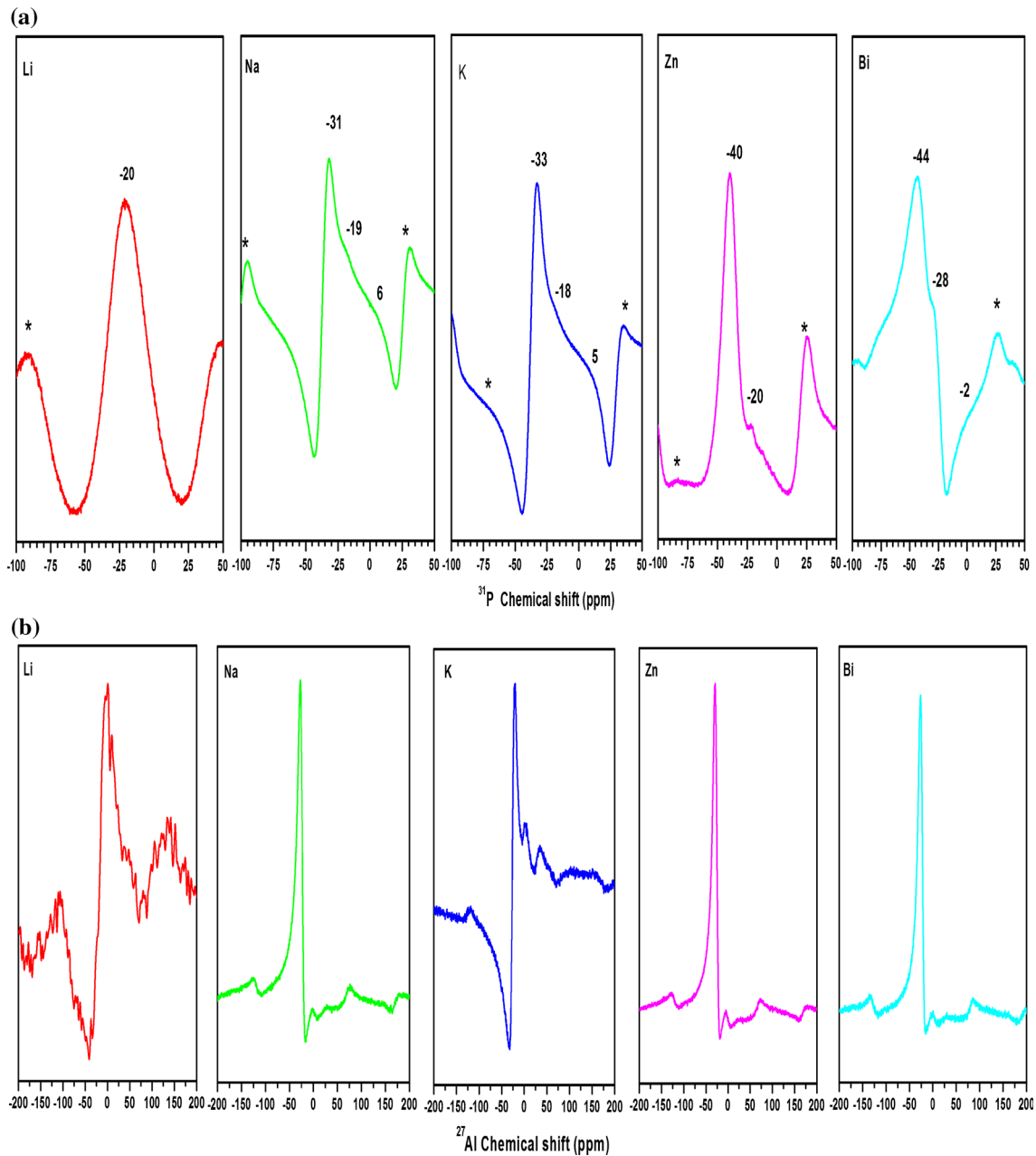


Figure 4 a ³¹P, b ²⁷Al MAS NMR spectra of different FP host glasses.

Table 2 ^{31}P MAS NMR spectra of different fluoro-phosphate host glasses

Glass	Chemical shift δ (ppm)	Units
Li	-20	Q^2
Na	-31	Q^2
	-19	Q^1
	6	Q^0
K	-33	Q^2
	-18	Q^1
	5	Q^0
Zn	-40	Q^3
	-20	Q^2
Bi	-44	Q^3
	-28	Q^2
	-2	Q^0

lithium FP glass was dominated by the major signal of Q^2 units (phosphate tetrahedral with two bridge oxygens) with chemical shift of about -20 ppm, and others were sidebands arise due to anisotropic shifts (Table 2). These units were related to metaphosphate units. The signal had a sort of single symmetric peak, which indicates the existence of no other Q^0 , Q^1 , and Q^3 structural units. The absence of these structural units in lithium FP glass matrix was due to the availability of sufficient quantity of oxygen bonds. The observed large linewidths indicate the formation of non-crystalline state of the prepared glasses. It was observed that Li, Na, K, Zn, and Bi FP glasses exhibit strong signal with chemical shifts -20, -31, -33, -40, and -44 ppm, respectively. With the modification in the modifier oxide, chemical shifts became more negative. The NMR shifts were found sensitive to the local environment. As more cross connections are formed in the glass, the charge on the oxygen had moved away from the P-O bonds, running to the nuclei becoming more shielded, producing a change in chemical shift and lead to increased network connectivity. It could thus be distinctly stated that modifier ions are connected (P-O-M, M = Li, Na, K, Zn, Bi) exclusively to the phosphate group. The structural depolymerization was observed from lithium FP glass matrix to bismuth FP glass matrix through the appearance of other structural units (Q^1 , Q^3). This observation is coherent with the Raman spectral analysis also [16–21].

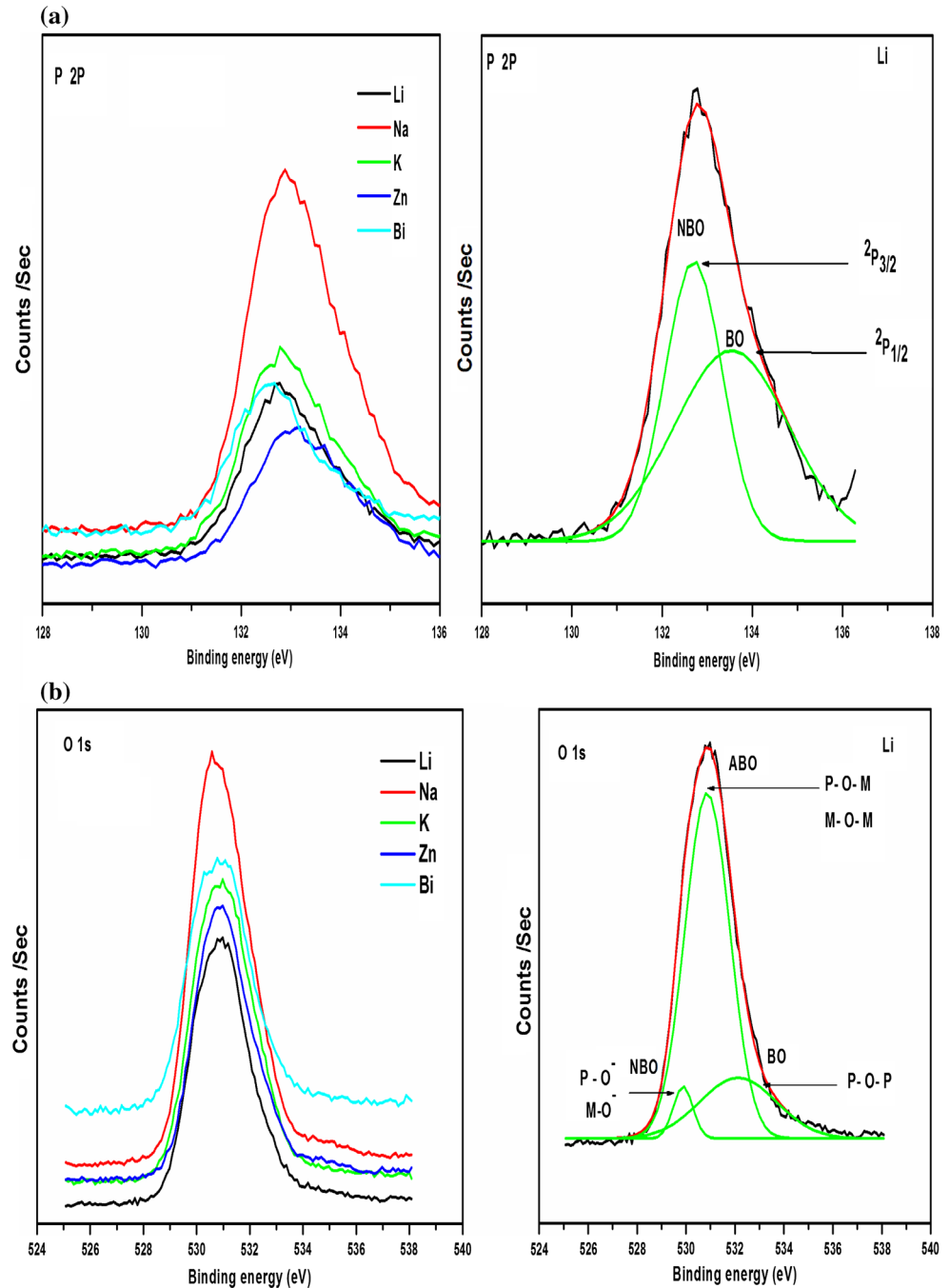
From Fig. 4b, it is observed that Li, Na, K, Zn, and Bi FP glasses show intense resonance signals at 2, -27, -21, -30, and -36 ppm, respectively. Most of the peaks are assigned due to the octahedrally

coordinated Al. Hence, all the prepared glasses tend to co-ordinate in the Al(6) structure except lithium FP glass matrix [22]. In the case of lithium FP glass matrix, single resonance peak (2 ppm) was observed which could be assigned to Al(5) coordination of Al^{3+} ions based on the ^{27}Al NMR spectra. However, other glass matrices, consist of other additional peaks, i.e., Na (0, 6 ppm); K (-3, 33 ppm); Zn (-1, 26 ppm); and Bi (0, 28 ppm). These additional peaks in the regions -1 to -3 ppm and 6–33 ppm were assumed to be Al(5) and Al(4) structural units [23, 24]. All these glass matrices had symmetric in resonance peak, which suggests that there are no other dominated structural coordination units. Hence, they have coordinated to other atoms in order to satisfy charge compensation.

X-ray photoelectron spectroscopy (XPS)

The binding energy (B.E.) of the core level spectra is very informative in terms of the structural role of cations occupy in glass host. The deconvolution of the P 2p spectra into two peaks could arise from the spin-orbit splitting of the P 2p core level, resulting in the distinguishable $\text{P } 2\text{P}_{3/2}$ and $\text{P } 2\text{P}_{1/2}$ core levels with the lower and higher binding energy peaks, respectively. Such fitting for lithium FP glass matrix is depicted in Fig. 5a. Oxygen atoms were found more covalently bonded to phosphate units on both sides. This formation could be called as bridging oxygens (BO) (133.5 eV) like P-O-P, M-O-M, and P-O-M (M = Al, Ba, Sr, Pb, Li, Na, K Zn and Bi). Oxygen atoms were more ionically bonded (double bonded) to phosphate units were referred to as non-bridging oxygen (NBO) atoms like P=O bonding (132.7 eV). Bridging and non-bridging oxygens had higher and lower binding energies, respectively. The B.E. values in the prepared FP glasses centered at 132.7 eV suggest that due to the O-P-O bonding of the PO_4^{2-} , mode corresponds to the metal-phosphate network [25]. The presence of non-bridging oxygens have indicated more than one valence states such as Sr^{2+} and Al^{3+} linked to phosphate units. The first component with B.E. 133.5 eV ($\text{P } 2\text{P}_{1/2}$) could be attributed to pentavalent tetra-coordinated phosphorus units (pyrophosphate and orthophosphate) surrounded by different chemical environments. The second component observed in P 2p spectrum with B.E. 132.7 eV ($\text{P } 2\text{P}_{3/2}$) should be attributed to the remaining metaphosphate units [26, 27].

Figure 5 a P 2p XPS spectra of different FP host glasses
b O 1s XPS spectra of different FP host glasses.



The deconvoluted spectrum of O 1s for lithium FP glass matrix is presented in Fig. 5b. The peak located at higher B.E. related to BO in P–O–P binding, while peak located at lower B.E. related to NBO coming from P–O⁻ and M–O⁻. From XPS spectrum, it is observed that in between bridging and non-bridging oxygens, asymmetric bridging oxygens (ABO) are present due to the formation of P–O–M

and M–O–M bondings. The BE energy of NBO O 1s spectra was lower than that of ABO bonding. The fraction of BO and NBO were very less. The dominated peak represents asymmetric bridging oxygen group in all the FP glasses. The peak profile of core level spectra was found independent of glass host composition. But the variation in intensity was observed.

DSC analysis

DSC curves were recorded for all FP host glass matrices and are shown in Fig. 6a–e. The temperatures of glass transition (T_g) and crystallization (T_C) corresponding to endothermic and exothermic peaks were obtained from these figures. The difference in T_g and T_C was used to measure the thermal stability (ΔT) or the glass forming ability or measure of its disorder in glassy state of host glass matrices. In between this temperature interval, the nucleation process takes

place. From DSC analysis, it was observed that the glass transition temperatures (T_g) were 305, 306, 307, 304, and 300 °C for the Li, Na, K, Zn, and Bi FP glasses, respectively. The crystallization temperatures were found to be 380, 382, 393, 404 and 430 °C for the Li, Na, K, Zn, and Bi FP glasses, respectively. The thermal stability parameters were found to be 75, 76, 86, 100, and 130 °C for the Li, Na, K, Zn, and Bi FP glasses, respectively. ΔT value changes with respect to compositional change. The better thermal stability ($\Delta T > 100$ °C) is found in the case of bismuth FP glass

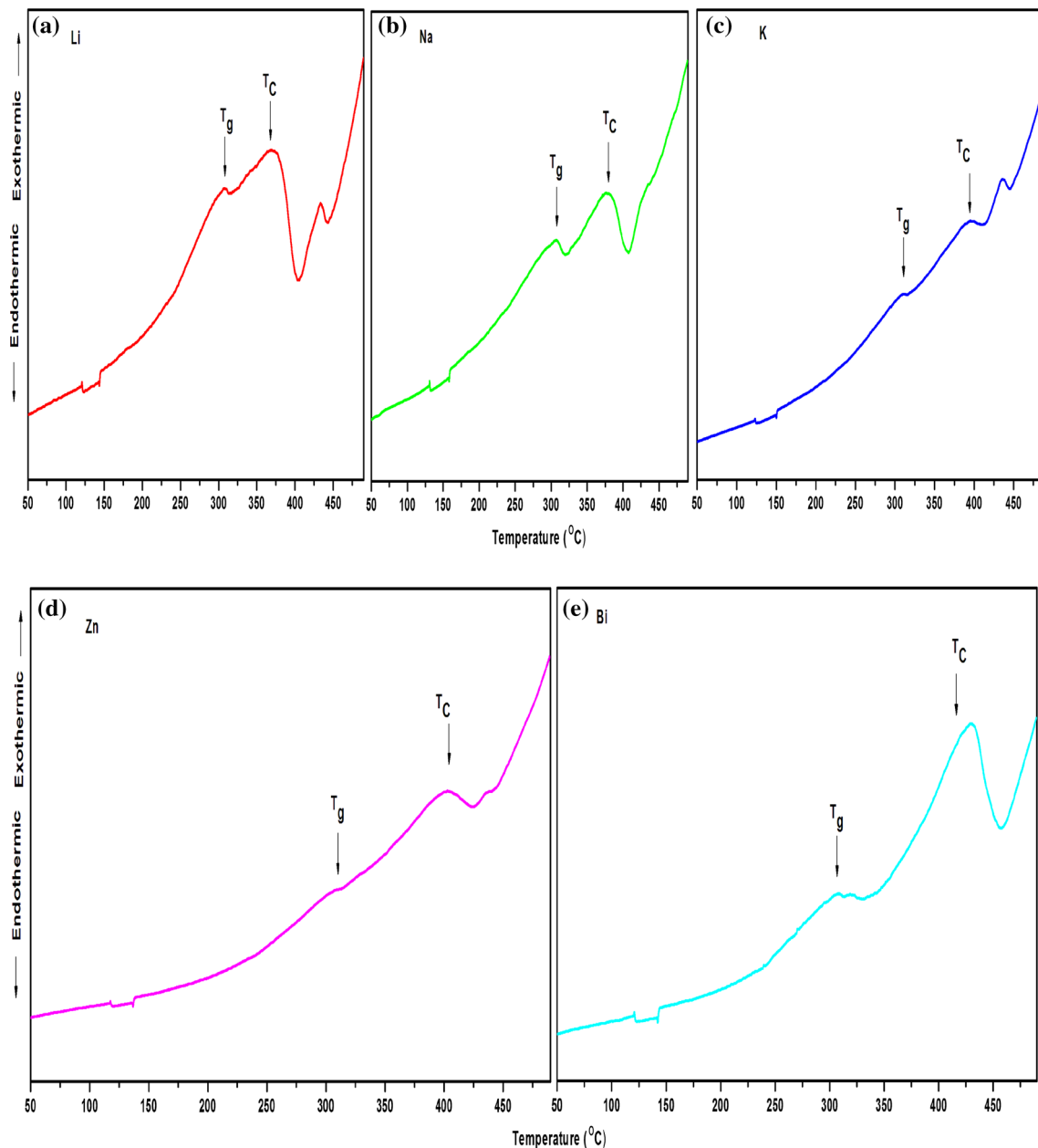


Figure 6 DSC thermal profiles for the a Li, b Na, c K, d Zn, and e Bi FP host glass matrix.

(130 °C) than that in the other FP glasses. The higher thermal stability of the present bismuth FP glass system was due to the shifting of symmetric stretching of O–P–O non-bridge oxygen atoms of phosphate group which would require large thermal energy. Glasses which have more disordered structural units were found to have higher ΔT magnitudes. When stability parameter (ΔT) magnitude is low, the thermal energy needed to crystallize a glass system is also low.

Dielectric properties

The real (ϵ') and imaginary (ϵ'') parts of complex dielectric constant were obtained from the expression [28]

$$\epsilon^*(\omega) = \epsilon'(\omega) + j\epsilon''(\omega)$$

$$\epsilon' = C_p t / A \epsilon_0$$

$$\epsilon'' = \epsilon' \tan \delta$$

The temperature dependence of ϵ' for lithium FP host glasses at selected frequencies is shown in Fig. 7. It can be noticed from the figure that the rate of dielectric constant with temperature decreases slowly up to the 80 °C, and after that, it has increased rapidly in all FP glasses. This behavior was typical to the polar dielectrics in which the orientation of dipoles was facilitated with rising temperature, and therefore the dielectric constant is increased. At low temperatures, the contribution of electronic and ionic components to the total polarizability will be small. As the temperature has increased, the electronic and ionic polarizabilities start to increase. The observed

increase in dielectric parameters at higher temperatures was due to large surface charge polarization near electrodes.

With the increase in frequency above 1 kHz, the dielectric constant decreases. At lower frequency, the dipoles align themselves along the applied field and contribute effectively to the total polarization. At higher frequency, variation in the applied field was too fast for the dipoles and unable to rotate freely. Higher magnitude of ϵ' at lower frequency and lower magnitude of ϵ' at higher frequency was observed for all the FP glasses. The dielectric constants found at 1 kHz are 0.05, 0.09, 0.10, 0.12, and 0.20 for the Li, Na, K, Zn, and Bi FP glasses, respectively. The magnitude of ϵ' was higher at bismuth and lower at lithium FP glasses. These changes in magnitude were due to the increase in depolymerization of phosphate network from lithium to bismuth FP glasses which was noticed from Raman and ^{31}P NMR data. This depolymerization process increases the large number of non-bridge oxygen's, i.e., free ions and effectively contribute for the increase in dielectric constant ϵ' . Hence, bismuth-based glass system shows higher dielectric constant. The variation of dielectric loss $\tan \delta$ exhibited the same trend as was observed in the case of dielectric constant with temperature, and for the lithium, FP host glass matrix is shown in Fig. 8. It was noticed that the dielectric loss has decreased with an increase in the frequency [29–31].

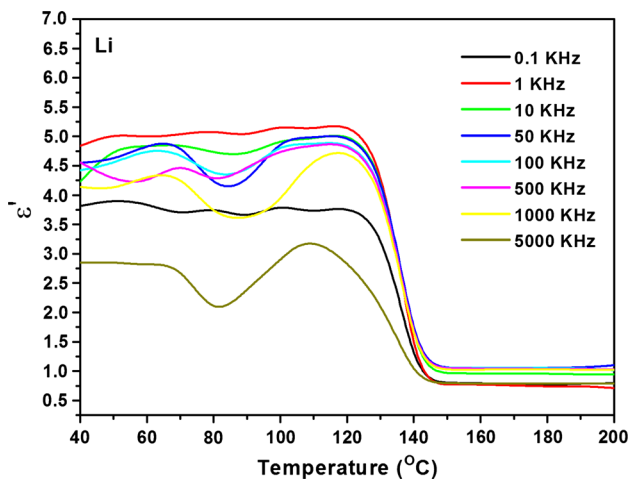


Figure 7 The temperature dependence dielectric constant of lithium FP host glass matrix at different frequencies.

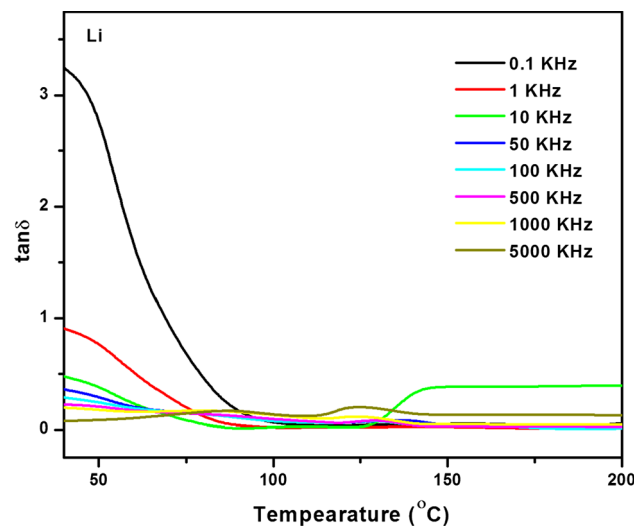


Figure 8 The temperature dependence dielectric loss of lithium FP host glass matrix at different frequencies.

Electrical properties

Impedance spectroscopy is a good technique for characterizing electric behavior of a material. Real (Z') and imaginary (Z'') parts of impedance can be expressed as [32, 33]

$$Z' = |Z| \cos \theta \quad Z'' = |Z| \sin \theta,$$

where θ is the phase angle. The obtained electrical conductivity data were explained by the means of frequency-dependent conductivity spectra. Figures 9a–e show the impedance spectra for different FP glasses at selected temperatures. From the figure (Cole–Cole plots), it was observed that lithium FP glass matrix had single semicircle which was electronic in nature. Similar results were observed in the case of sodium and zinc FP glass matrices. The bulk resistance (R) of the glass sample was obtained from the intercept of the imaginary Z'' impedance with real Z' impedance axes. The resistance (R) and area (A) was used to calculate bulk conductivity of the FP glasses at given temperature, i.e., dc electrical conductivity (σ_{dc}) [34]:

$$\sigma_{dc} = 1/\rho_{dc} = (1/R)(t/A),$$

where σ_{dc} is direct current electrical conductivity, R is the resistance in ohms, t/A is sample geometric ratio, t is the thickness of glass sample in cms, and A is the electrode surface area in cms. From Fig. 9a (for lithium FP), it was observed that the semicircle intercepts the abscissa at higher Z'' values with the increasing temperature, indicating the decrease in dc conductivity. With the increasing temperature, Z'' value increased up to 80 °C. As the thermal energy given to the material was gradually increased, the charge carriers are unable to overcome the binding energy. Above 80 °C, straight line appears in the graph, indicating the behavior of insulator. The appearance of semicircle and straight lines in the same glass material indicates the presence of both localized and non-localized conduction process [35]. The resistance values were found to be 1.5, 2.4, and 15.3 M Ω at 40, 60, and 80 °C temperatures for lithium FP glass matrix, respectively. Sodium and potassium FP glass matrices have exhibited straight line in Cole–Cole plots at ≥ 60 °C. Potassium and bismuth FP glass matrices exhibited straight lines ≥ 40 °C, indicating the behavior of insulator. Among all the glass matrices, lithium has exhibited higher σ_{dc} conductivity (5.29×10^{-8} S cm $^{-1}$) and zinc has exhibited lower σ_{dc} conductivity (0.15×10^{-8} S cm $^{-1}$).

X-ray absorption near-edge spectroscopy (XANES)

Figure 10 shows the XANES spectra of praseodymium-doped glass samples at Pr L3 absorption edge along with Pr₆O₁₁ standard. From the figure, it was observed that the XANES spectra of the all praseodymium-doped samples had similar peak positions despite the different glass compositions. However, the white line intensity was found different for each of the FP glass samples. None of the XANES spectra matched with the standard spectra of Pr₆O₁₁, which shows that the Pr cation environment in the doped glass sample was quite different from that in the Pr₆O₁₁ standard. Standard or pure Pr₆O₁₁ had two peaks. One was higher photon energy side (6024 eV), related to higher oxidation state (Pr⁴⁺), and another one was lower photon energy side (6012 eV), related to lower oxidation state (Pr³⁺). As one could expect, a fraction of Pr⁴⁺ is reduced to stable Pr³⁺, and edge position remains constant upon doping into the FP glass system. The XANES spectra had a pre-edge (6044 eV) which might be the result of an asymmetric or static disorder arrangement of atoms around Pr cations [36, 37].

Absorption spectroscopy and J–O theory

Figures 11a, b represents the absorption spectra for Pr³⁺-doped different FP glasses [38]. The absorptions takes place from the ground state, ³H₄, to various excited states which are shown in Fig. 11a, b. The most intense absorption bands were found in the spectral range 400–500 nm. In this range, the intense absorption bands observed at 444, 469, and 481 nm were assigned to the transitions ³H₄ → ³P₂, ³P₁ + ¹I₆, and ³H₄ → ³P₀, respectively. The weak bands observed at 589 and 1011 nm were attributed to the ³H₄ → ¹D₂ and ³H₄ → ¹G₄ transitions, respectively. The overlapped broad absorption peak at 1520 nm was assigned to the ³H₄ → ³F₄ + ³F₃ transition. The relatively intensive absorption band at 1941 nm was assigned to the ³H₄ → ³F₂ transition. One very weak absorption band in the NIR spectral range at 2230 nm was assigned to the ³H₄ → ³H₆ transition. All these transitions were mainly electric dipole in nature and only the ³H₄ → ¹G₄, ³F_{4/3} transitions had a small magnetic dipole character. Analysis of experimental absorption spectra of Pr³⁺ doped FP glasses was performed using J–O theory [39, 40].

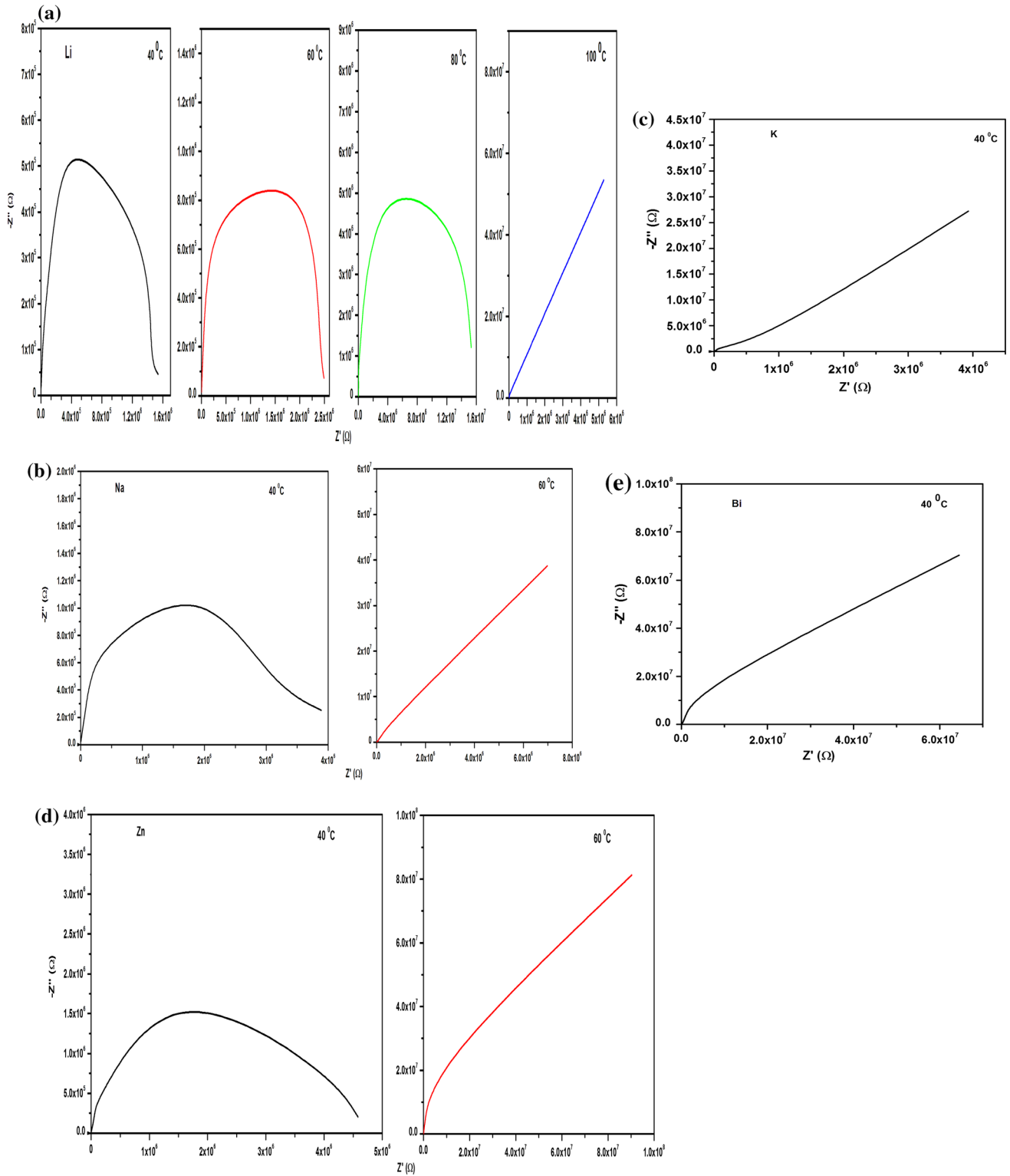


Figure 9 The complex plane plot of the impedance ($-Z''/Z'$) for the **a** Li, **b** Na, **c** K, **d** Zn, and **e** Bi fluoro-phosphate host glass matrix at different temperatures.

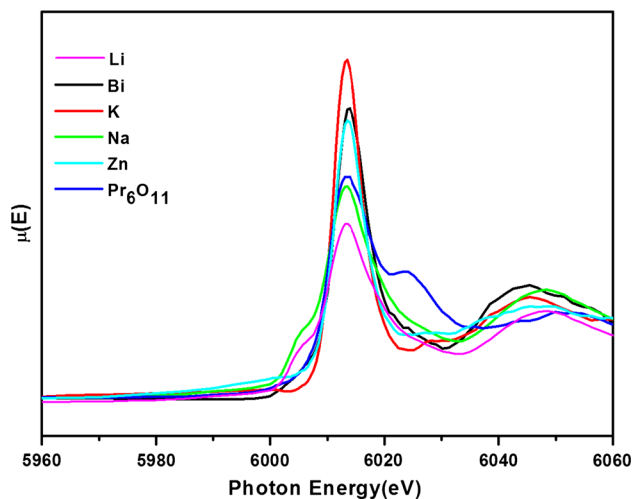


Figure 10 XANES spectra of standard praseodymium and Pr^{3+} doped different fluoro-phosphate glasses.

Table 3 shows the spectral intensities of different absorption bands of Pr^{3+} ion for lithium FP glass system. The difference between experimental and calculated spectral intensity of excited state for $^3\text{P}_2$ was found high, and the average RMS deviation was calculated at ± 0.87 . This anomalous behavior of this transition was due to the small energy difference between the ground-state configuration $4f^2$ and the first excited state configuration $4f^15d^1$. The deviation is observed in many hosts [5, 41, 42]. Among different transitions, the transitions $^3\text{H}_4 \rightarrow ^3\text{P}_2$ (in visible region) and $^3\text{H}_4 \rightarrow ^3\text{F}_3$ (in NIR region) had higher spectral intensity in all FP glasses. Some of the spectral intensities have sensitive character to the small change in the surrounding environment. These transitions are called ‘hypersensitive transitions.’ These transitions obey the selection rules, $|\Delta J| \leq 2$, $|\Delta L| \leq 2$ and $\Delta S = 0$, which are the same as those of a pure quadrupole transition [43]. The transition, $^3\text{H}_4 \rightarrow ^3\text{P}_2$, was the hypersensitive transition for the praseodymium ion, and the transition intensity changed significantly with the glass composition.

The J–O parameters were obtained from the least square approach, and the results are summarized in Table 4 along with other hosts. The Ω_2 parameter strongly depends on short range effects, such as covalency of the RE ion and sensitive to the symmetry of RE ion site, while Ω_4 and Ω_6 are long-range parameters related to the bulk properties of the glass such as rigidity and viscosity [44]. Covalency was found to decrease in the order $\text{Li} \rightarrow \text{Na} \rightarrow$

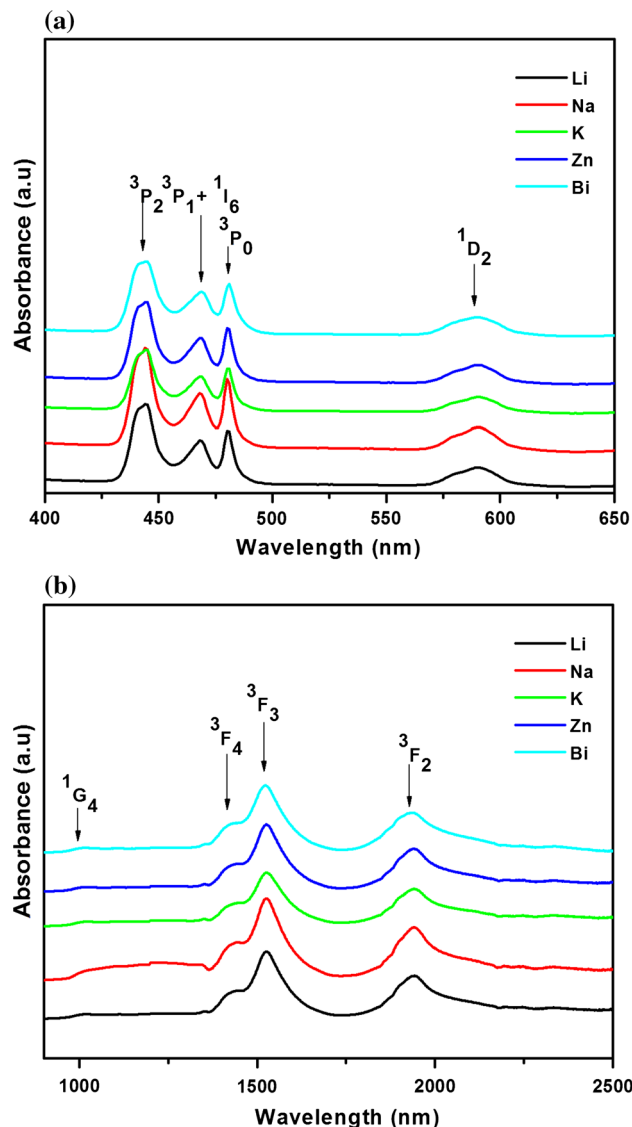


Figure 11 a UV–Vis and b NIR absorption spectra of Pr^{3+} -doped different fluoro-phosphate glasses.

$\text{Zn} \rightarrow \text{K} \rightarrow \text{Bi}$ in Pr^{3+} -doped FP glasses. The obtained value of Ω_2 parameter in lithium FP glass of $4.86 \times 10^{-20} \text{ cm}^2$ was found higher than that in phosphate [45], ZBLAN [46], fluoride [47], and FP glasses [48], indicating the higher asymmetry/higher covalency and lower covalency, compared with chalcogenide [49] and fluorotellurite [50] glasses, respectively.

Radiative properties

The J–O intensity parameters (Ω_λ) are widely used to estimate certain radiative properties and to predict

Table 3 Experimental (f_{exp}) and calculated (f_{cal}) spectral intensities ($\times 10^{-5}$) of Pr^{3+} -doped lithium fluoro-phosphate glass matrix

S. no.	Transition	Li	
		f_{exp}	f_{cal}
1	$^3\text{P}_2$	6.15	1.29
2	$^3\text{P}_1 + ^1\text{I}_6$	1.90	2.41
3	$^3\text{P}_0$	1.67	1.69
4	$^1\text{D}_2$	0.55	0.40
5	$^1\text{G}_4$	0.10	0.11
6	$^3\text{F}_4$	0.90	1.18
7	$^3\text{F}_3$	2.58	2.49
8	$^3\text{F}_2$	1.39	1.39
RMS deviation		± 0.87	

luminescence characteristics of certain transitions. Radiative properties such as total radiative transition probabilities (A_T), radiative lifetimes (τ_R), branching ratios (β_R), and absorption cross sections (Σ) for the excited states and $^3\text{P}_1$, $^3\text{P}_0$, $^1\text{D}_2$, and $^3\text{F}_3$ of Pr^{3+} -doped different FP glasses are estimated. Among various states, radiative transition probability was found to be in the order of $^3\text{P}_0 > ^3\text{P}_1 > ^1\text{D}_2 > ^3\text{F}_3$ in all FP glasses (Table 5). The state, $^3\text{P}_0$ had higher transition probability, i.e., 17525 s^{-1} in lithium FP glass matrix. Higher emission probability caused the faster decay of that emission level and hence reduction of the lifetime (τ_R). Among all the excited states, $^3\text{F}_3$ state had higher radiative lifetimes was observed. Among various transitions, the transitions, $^3\text{P}_1 \rightarrow ^3\text{H}_5$, $^3\text{P}_0 \rightarrow ^3\text{H}_4$, $^1\text{D}_2 \rightarrow ^3\text{H}_4$, and $^3\text{F}_3 \rightarrow ^3\text{H}_4$, have higher magnitude of integrated absorption cross sections and also predicted branching ratios (from J–O theory) in all FP glasses. Among different FP glasses, lithium FP glass matrix has higher Σ values for the transition $^3\text{P}_0 \rightarrow ^3\text{H}_4$ i.e., $133.6 \times 10^{-16} \text{ cm}^{-1}$. For the remaining

Table 4 J–O intensity parameters ($\Omega_\lambda, \times 10^{-20} \text{ cm}^2$) of Pr^{3+} -doped different fluoro-phosphate glasses

Glass	Ω_2	Ω_4	Ω_6	Trend	References
Li	4.86	2.60	1.65	$\Omega_2 > \Omega_4 > \Omega_6$	Present work
Na	4.36	2.27	2.45	$\Omega_2 > \Omega_6 > \Omega_4$	Present work
K	2.87	2.40	1.81	$\Omega_2 > \Omega_4 > \Omega_6$	Present work
Zn	4.08	2.29	2.49	$\Omega_2 > \Omega_6 > \Omega_4$	Present work
Bi	2.86	1.92	1.71	$\Omega_2 > \Omega_4 > \Omega_6$	Present work
Phosphate	3.42	4.09	4.35	$\Omega_6 > \Omega_4 > \Omega_2$	[45]
ZBLAN	2.44	4.41	5.52	$\Omega_6 > \Omega_4 > \Omega_2$	[46]
Fluoride	2.50	5.40	6.00	$\Omega_6 > \Omega_4 > \Omega_2$	[47]
Fluoro-phosphate	2.75	3.21	3.36	$\Omega_6 > \Omega_4 > \Omega_2$	[48]
Chalcogen	9.11	7.50	5.66	$\Omega_2 > \Omega_4 > \Omega_6$	[49]
Fluorotellurite	4.76	3.00	5.50	$\Omega_6 > \Omega_2 > \Omega_4$	[6]

Table 5 Total radiative transition probability (A_T) (s^{-1}) and radiative lifetime (τ_R) (μs) of certain excited states of Pr^{3+} -doped different fluoro-phosphate glasses

Glass	$^3\text{P}_1$		$^3\text{P}_0$		$^1\text{D}_2$		$^3\text{F}_3$	
	A_T	τ_R	A_T	τ_R	A_T	τ_R	A_T	τ_R
Li	16465	60	17525	57	11561	86	2810	355
Na	15624	64	16305	61	12011	83	3274	305
K	15076	66	15913	62	10470	95	2788	358
Zn	15826	63	16507	60	12082	82	3325	300
Bi	12558	79	13187	75	9133	109	2460	406

glass matrices, i.e., Na, K, Zn, and Bi FP glasses, Σ values are 116.6×10^{-16} , 123.2×10^{-16} , 118.7×10^{-16} , and $98.4 \times 10^{-16} \text{ cm}^{-1}$, respectively, for the transition $^3\text{P}_0 \rightarrow ^3\text{H}_4$. Another important radiative property, the fluorescent branching ratios, β_R , for different emissions levels were calculated and observed that the transition, $^3\text{P}_0 \rightarrow ^3\text{H}_4$, had higher radiative branching ratios (66, 62, 67, 62, and 65 %) for the Li, Na, K, Zn, and Bi FP glass matrices, respectively.

Emission analysis

Under the excitation energy 443 nm wavelength, Pr^{3+} ions are quickly transferred from the ground state to the higher excited state, $^3\text{P}_0$. Because of the small energy gap between the $^3\text{P}_0$ level and to the next lower level $^1\text{D}_2$, these two levels were thermalized at room temperature. Hence, emission took place from these two excited levels. It was worth to note that the remarking that the multiphonon relaxation processes from higher level to next lower $^1\text{D}_2$ level was found efficient due to small energy gap. Moreover, the gap between the $^1\text{D}_2$ level and the next level, $^1\text{G}_4$ is larger,

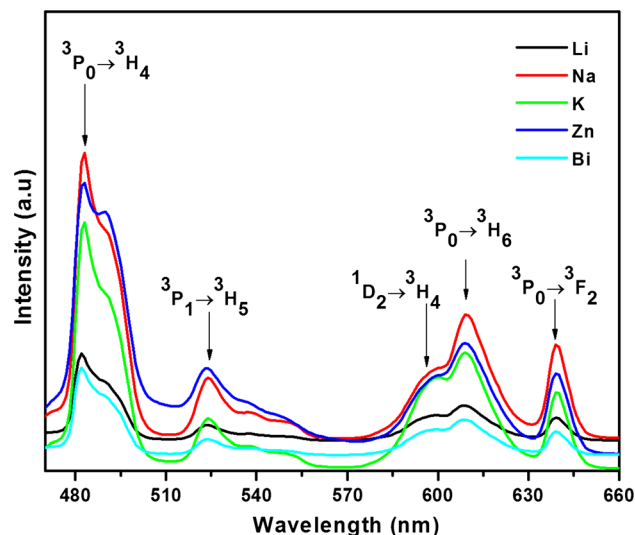


Figure 12 Emission spectra of Pr^{3+} -doped different fluoro-phosphate glasses.

nearly 7000 cm^{-1} , more phonons are required to bridge the energy gap. Therefore, radiative emission from the both $^3\text{P}_0$ and $^1\text{D}_2$ levels to lower ground state is very high. Two bands corresponding to the transitions $^3\text{P}_0 \rightarrow ^3\text{H}_4$ (482 nm) and $^3\text{P}_0 \rightarrow ^3\text{H}_6$ (610 nm) were considerably more intense than the other bands related to $^3\text{P}_1 \rightarrow ^3\text{H}_5$ (525 nm), $^1\text{D}_2 \rightarrow ^3\text{H}_4$ (595 nm) and $^3\text{P}_0 \rightarrow ^3\text{F}_2$ (645 nm) [51]. It was worth to note that the intensities of two emission transitions were much stronger. However, the spectral shape of this peak was the same for different glasses and not normally depend on their chemical compositions (Fig. 12).

Luminescence parameters for the two prominent emission transitions were calculated for all the glass matrices and are shown in Table 6. It is noted that the transition, $^3\text{P}_0 \rightarrow ^3\text{H}_4$, of Pr^{3+} was the most probable emission transition than the transition $^3\text{P}_0 \rightarrow ^3\text{H}_6$.

Table 6 Emission band positions (λ_p , nm), radiative transition probabilities (A s^{-1}), peak stimulated emission cross-sections (σ_p , $\times 10^{-20} \text{ cm}^2$), and branching ratios (β_{exp} %) of prominent emission transitions of Pr^{3+} -doped different fluoro-phosphate glasses

S.no.	Transition	Parameters	Li	Na	K	Zn	Bi
1	$^3\text{P}_0 \rightarrow ^3\text{H}_4$	λ_p	482	482	482	482	482
		A_R	11609	10334	10707	10132	8576
		σ_p	2.19	2.28	1.94	1.46	1.18
		β_{exp}	39	46	41	45	37
2	$^3\text{P}_0 \rightarrow ^3\text{H}_6$	λ_p	610	610	610	610	610
		A_R	1582	2349	1745	2392	1648
		σ_p	0.77	1.34	1.26	0.86	0.68
		β_{exp}	19	21	22	21	22

Also, it was noted that the predicted radiative transition probability for the transition $^3\text{P}_0 \rightarrow ^3\text{H}_4$ of Pr^{3+} -doped sodium FP glass (which has high emission intensity) was 10334 s^{-1} , which was higher than another kinds of fluorotellurite glass (4576 s^{-1}) [6] and borate glass (1318 s^{-1}) [7], and lower than phosphate (30380 s^{-1}) [52] and tellurite (56348 s^{-1}) [53]. Higher spontaneous emission probability provides better opportunity to obtain laser actions. The fluorescence branching ratio is a significant factor to any optical material, because it characterizes the possibility of attaining fluorescence from any specific transitions. Among different transitions, branching ratio of $^3\text{P}_0 \rightarrow ^3\text{H}_4$ emission transition was found the highest one. Therefore, this transition could be considered as good fluorescent transition. Further, the magnitude of β parameter was higher for the sodium FP glass matrix (46 %) and lower (37 %) for bismuth FP glass matrix. Hence, sodium FP glass could be considered as more appropriate for lasing material.

The stimulated emission cross section (σ_p) of emission transition is one of the important parameters used to identify a good optical material. A good optical material has a large emission cross section. It was observed that the transition, $^3\text{P}_0 \rightarrow ^3\text{H}_4$, showed higher peak emission cross section, i.e., $2.28 \times 10^{-20} \text{ cm}^2$ at $\lambda_p = 482 \text{ nm}$ in sodium FP glass (which had high emission intensity) which was higher compared with typical values reported in the literature for other borate ($1.24 \times 10^{-20} \text{ cm}^2$) [54] and lower magnitude than phosphate ($5.54 \times 10^{-20} \text{ cm}^2$) [52] glasses.

Decay curve analysis

Fluorescence decay profiles of $^3\text{P}_0$ level of Pr^{3+} -doped different FP glasses were recorded (λ_{ex} : 443 and λ_{em} :

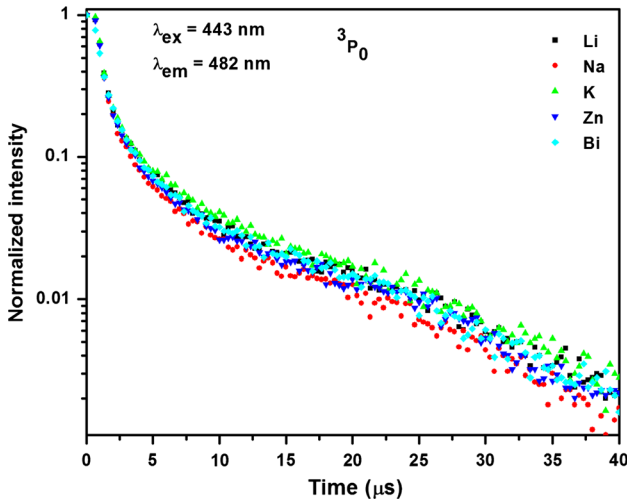


Figure 13 Decay profiles of Pr³⁺ doped different fluoro-phosphate glasses for the ³P₀ level.

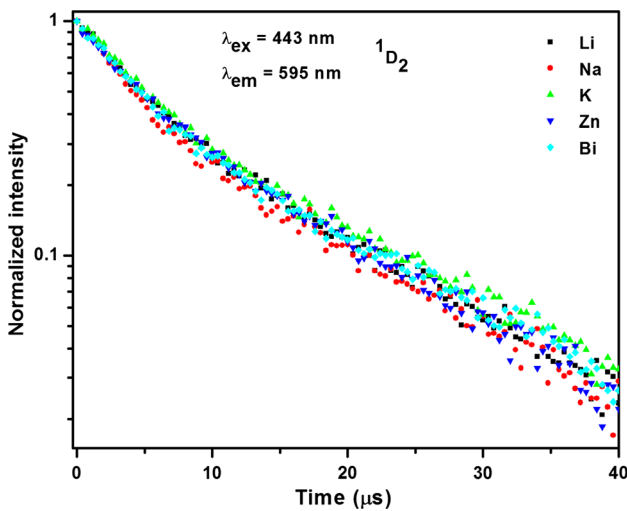


Figure 14 Decay profiles of Pr³⁺ doped different fluoro-phosphate glasses for the ¹D₂ level.

482 nm) and are shown in Fig. 13. All the curves were fitted to bi-exponential function due to the hydrophilicity content of OH groups in phosphate glasses and were found to be higher than in silicate, borate, and tellurite glasses. The coordination of water molecules produce the severe vibration of the hydroxyl group, resulting in the large non-radiative transition and decreasing luminescence efficiency. In the present work, the average lifetime decay constants for ³P₀ excited state were found to be 10, 11, 10, 10, and 11 μs for Li, Na, K, Zn, and Bi FP glasses, respectively. It was observed that large variation of

glass composition did not influence the measured lifetimes. Fluorescence decay profiles of ¹D₂ level of Pr³⁺-doped different FP glasses were recorded (λ_{ex}: 443 and λ_{em}: 595 nm) and are shown in Fig. 14. All the decay profiles were fitted to bi-exponential function. The lifetimes were found to be 15, 16, 17, 15, and 14 μs for the lithium, sodium, potassium, zinc, and bismuth FP glasses, respectively. It is observed that with change in the glass composition, the lifetimes were increased in the order lithium > sodium > potassium glass matrices, whereas for zinc and bismuth, the lifetimes are decreased for this level. The lifetimes were longer for the ¹D₂ level than ³P₀ level. In the present work, lifetimes were found to be 14–17 μs range and reasonable agreement with other reported lead borate glass [55] and shorter than that of lead telluroborate [56] and borate [54] glasses.

Conclusions

Pr³⁺-doped different FP glasses were found to be homogeneous and amorphous in nature, as confirmed by X-ray diffraction patterns and SEM. FTIR and Raman spectra of the studied FP glasses contain typical phosphate bonds. Phosphate acted as a network former. All metal oxides entered into the glass structure as network modifiers. Bi₂O₃ was incorporated in the form of BiO₃ and BiO₆ octahedra into glass structure as confirmed by the characteristic Raman band at 273 cm⁻¹. On the basis of ³¹P MAS NMR analysis, a decrease in the proportion of Q² units in the sequence Li → Na → K → Zn → Bi in these FP host glasses was observed which indicates that these oxides were incorporated into glass as network modifier oxides. The better thermal stability (ΔT > 100 °C) is found in the case of bismuth FP glass (130 °C) than that in the other FP glasses. The dielectric constants at 1 kHz were found to be 0.05, 0.09, 0.10, 0.12, and 0.20 for the Li, Na, K, Zn, and Bi FP glasses respectively. The magnitude of ε' was higher for bismuth and lower for lithium FP glasses. Among all the glass matrices, lithium exhibits higher σ_{dc} conductivity (5.29 × 10⁻⁸ S cm⁻¹) and zinc exhibits lower σ_{dc} conductivity (0.15 × 10⁻⁸ S cm⁻¹). From XANES spectra, it was established that the prepared Pr doped glasses had +3 as oxidation state. Among the three J–O intensity parameters in all the FP glasses, the magnitude of Ω₂ parameter was

higher in lithium FP glass which could be attributed to higher covalency and asymmetry in this glass matrix. Among various states, radiative transition probability was decreasing in the order of ${}^3P_0 > {}^3P_1 > {}^1D_2 > {}^3F_3$ in all FP glasses. We conclude from above several spectroscopic characterizations that sodium FP glass is to be considered as an appropriate candidate for the bright blue luminescent intensity (${}^3P_0 \rightarrow {}^3H_4$ at 482 nm). This observation agrees with the results from higher luminescence intensities, higher radiative transition probabilities, higher emission cross sections, and more branching ratios.

Acknowledgements

One of the authors S. Babu would like to thank University Grants Commission (UGC), New Delhi for the sanction of Senior Research Fellowship (SRF) under Research Fellowship in Sciences for Meritorious students (RFSMS) scheme. The authors are thankful to Dr. S.N. Jha, Scientific officer (SOH), A&MPD, BARC, Mumbai for providing EXAFS measurements. The support of Dr. C. Nayak, Scientific officer (SOD), A&MPD, BARC, Mumbai to analyze the data is gratefully acknowledged.

References

- [1] Som T, Karmakar B (2011) Nephelauxetic effect of low phonon antimony oxide glass in absorption and photoluminescence of rare-earth ions. *Spectrochim Acta A* 79:1766–1782
- [2] Czaja M, Bodył S, Gabryś-Pisarska J, Mazurak Z (2009) Applications of Judd–Ofelt theory to praseodymium and samarium ions in phosphate glass. *Opt Mater* 31:1898–1901
- [3] Choi JH, Margaryan A, Margaryan A, Shi FG (2005) Judd–Ofelt analysis of spectroscopic properties of Nd^{3+} -doped novel fluorophosphate glass. *J Lumin* 114:167–177
- [4] Belkébir A, Rocha J, Esculcas AP, Berthet P, Gilbert B, Gabelica Z, Llabres G, Wijzen F, Rulmont A (1999) Structural characterization of glassy phases in the system $Na_2O-Al_2O_3-P_2O_5$ by MAS and solution NMR, EXAFS and vibrational spectroscopy. *Spectrochim Acta A* 55:1323–1336
- [5] Zhang YY, Chen BJ, Pun EYB, Lin H (2009) Optical radiative parameters and 1.3 μm emission anticipation of Pr^{3+} in two kinds of bismuth-containing oxide glasses with lower phonon energies. *Physica B* 404:1132–1136
- [6] Zhang F, Bi Z, Huang A, Xiao Z (2015) Luminescence and Judd–Ofelt analysis of the Pr^{3+} doped fluorotellurite glass. *J Lumin* 160:85–89
- [7] Anjaiah J, Laxmikanth C, Veeraiah N, Kistaiah P (2015) Luminescence properties of Pr^{3+} doped $Li_2O-MO-B_2O_3$ glasses. *J Lumin* 161:147–153
- [8] Gwizdala B, Reben M, Cisowski J, Lisiecki R, Romanowski WR, Jarzabek B, Mazurak Z, Nosidlak N, Grelowska I (2015) The influence of Pr^{3+} content on luminescence and optical behavior of $TeO_2-WO_3-PbO-Lu_2O_3$ glass. *Opt Mater* 31:1167–1172
- [9] Schwarz J, Tichá H, Tichý L, Mertens R (2004) physical properties of Pbo-Zno- P_2O_5 glasses I. Infrared and raman spectra. *J Optoelectron Adv Mater* 6:737–746
- [10] Zhang L, Sun H, Xu S, Zhang J, Hu L (2005) Special effects of YbF^{3+} on the structural changes for fluorophosphate glass. *Physica B* 367:1–5
- [11] Marzouk MA, ElBatal FH, Abdelghany AM (2013) Ultraviolet and infrared absorption spectra of Cr_2O_3 doped—Sodium metaphosphate, lead metaphosphate and zinc metaphosphate glasses and effects of gamma irradiation: a comparative study. *Spectrochim Acta A* 114:658–667
- [12] Li HW, Man SQ (2009) Optical properties of Er^{3+} in $MoO_3-Bi_2O_3-TeO_2$ glasses. *Opt Commun* 282:1579–1583
- [13] Hsu SM, Wu JJ, Yung SW, Chin TS, Zhang T, Lee YM, Chu CM, Ding JY (2012) Evaluation of chemical durability, thermal properties and structure characteristics of Nb–Sr-phosphate glasses by Raman and NMR spectroscopy. *J Non-Cryst Solids* 358:14–19
- [14] Poirier G, Messaddeq Y, Ribeiro SJ, Poulain M (2005) Structural study of tungstate fluorophosphate glasses by Raman and X-ray absorption spectroscopy. *J Solid State Chem* 178:1533–1538
- [15] Ivascuca C, Gabor AT, Cozar O, Daraban L, Ardelean I (2011) FT-IR, Raman and thermoluminescence investigation of $P_2O_5-BaO-Li_2O$ glass system. *J Mol Struct* 993:249–253
- [16] Sahar MR, Wahab A, Hussein MA, Hussin R (2007) Structural characteristic of $Na_2-P_2O_5-GeO_2$ glass systems. *J Non-Cryst Solids* 353:1134–1140
- [17] Kirkpatrick RJ, Brow RK (1995) Nuclear magnetic resonance investigation of the structures of phosphate and phosphate-containing glasses: a review. *Solid State Nucl Mag* 5:9–21
- [18] Weng CZ, Chen JH, Shih PY (2009) Effect of dehydroxylation on the structure and properties of $ZnCl_2-ZnO-P_2O_5$ glasses. *Mater Chem Phys* 115:628–631
- [19] Shih PY, Ding JY, Lee SY (2003) ${}^{31}P$ MAS-NMR and FTIR analyses on the structure of CuO-containing sodium poly- and meta-phosphate glasses. *Mater Chem Phys* 80:391–396

- [20] Qiu D, Guerry P, Ahmed I, Pickupa DM, Cartaa D, Knowles JC, Smithb ME, Newport RJ (2008) A high-energy X-ray diffraction, ^{31}P and ^{11}B solid-state NMR study of the structure of aged sodium borophosphate glasses. *Mater Chem Phys* 111:455–462
- [21] Wiench JW, Tischendorf B, Otaigbe JU, Pruski M (2002) Structure of polyphosphate glasses studied by two dimensional solid and liquid state NMR. *J Mol Struct* 602–603:145–157
- [22] Hsu SM, Yung SW, Brow RK, Hsu WL, Lu CC, Wu FB, Ching SH (2010) Effect of silver concentration on the silver-activated phosphate glass. *Mater Chem Phys* 123:172–176
- [23] Tiwari B, Pandey M, Sudarsan V, Deb SK, Kothiyal GP (2009) Study of structural modification of sodium aluminophosphate glasses with TiO_2 addition through Raman and NMR spectroscopy. *Physica B* 404:47–51
- [24] Gongyi G (1998) Structural study of a lead–barium–aluminum phosphate glass by MAS-NMR spectroscopy. *Solid State Nucl Mag* 13:119–122
- [25] Nagpure IM, Pitale SS, Coetsee E, Ntwaeaborwa OM, Terblans JJ, Swart HC (2012) Lattice site dependent cathodoluminescence behavior and surface chemical changes in a $\text{Sr}_5(\text{PO}_4)_3\text{F}$ host. *Physica B* 407:1505–1508
- [26] Majjane A, Chahine A, Et-tabirou M, Echchahed B, Do Trong-On, Mc Breen P (2014) X-ray photoelectron spectroscopy (XPS) and FTIR studies of vanadium barium phosphate glasses. *Mater Chem Phys* 143:779–787
- [27] Tshabalala MA, Dejene FB, Pitale SS, Swart HC, Ntwaeaborwa OM (2014) Generation of white-light from Dy^{3+} doped Sr_2SiO_4 phosphor. *Physica B* 439:126–129
- [28] Braunger ML, Escanhoela JA Jr, Fier I, Walmsley L, Ziemath EC (2012) Electrical conductivity of silicate glasses with tetravalent cations substituting Si. *J Non-Cryst Solids* 358:2855–2861
- [29] Ramteke DD, Gedam RS (2014) Study of $\text{Li}_2\text{O}-\text{B}_2\text{O}_3-\text{Dy}_2\text{O}_3$ glasses by impedance spectroscopy. *Solid State Ion* 258:82–87
- [30] Sdiri N, Elhouichet H, Dhaou H, Mokhtar F (2014) Effects of the substitution of P_2O_5 by B_2O_3 on the structure and dielectric properties in $(90-x)\text{P}_2\text{O}_5-x\text{B}_2\text{O}_3-10\text{Fe}_2\text{O}_3$ glasses. *Spectrochim Acta A* 117:309–314
- [31] Sambasiva Rao K, Srinivasa Reddy M, Ravi Kumar V, Veeraiah N (2008) Dielectric, magnetic and spectroscopic properties of $\text{Li}_2\text{O}-\text{WO}_3-\text{P}_2\text{O}_5$ glass system with Ag_2O as additive. *Mater Chem Phys* 111:283–292
- [32] Balaji Rao R, Gerhardt RA (2008) Effect of alkaline earth modifier ion on the optical, magnetic and electrical properties of lithium nickel borate glasses. *Mater Chem Phys* 112:186–197
- [33] Milankovi AM, Sklepi K, Blazanovi H, Mosner P, Vorokhta M, Koudelka L (2013) Influence of germanium oxide addition on the electrical properties of $\text{Li}_2\text{O}-\text{B}_2\text{O}_3-\text{P}_2\text{O}_5$ glasses. *J Power Sour* 242:91–98
- [34] Ahmad MM, Yousef ES, Moustafa ES (2006) Dielectric properties of the ternary $\text{TeO}_2/\text{Nb}_2\text{O}_5/\text{ZnO}$ glasses. *Physica B* 371:74–80
- [35] Sujatha B, Viswanatha B, Chethana BK, Nagabhushana H, Reddy CN (2016) Electrical conductivity and dielectric relaxation studies on microwave synthesized $\text{Na}_2\text{SO}_4\text{-NaPO}_3\text{-MoO}_3$ glasses. *Ionics* 22:563–571
- [36] Hormesa J, Pantelouris M, Balazs GB, Rambabu B (2000) X-ray absorption near edge structure (XANES) measurements of ceria-based solid electrolytes. *Solid State Ion* 136–137:945–954
- [37] Kiebach WR, Chatzichristodoulou C, Werchmeister RML, Hagen A (2012) Determination of redox-active centers in praseodymium doped ceria by in situ-XANES spectroscopy. *Chem Phys Lett* 537:80–83
- [38] Pal I, Agarwal A, Sanghi S, Aggarwal MP (2011) Structural, absorption and fluorescence spectral analysis of Pr^{3+} ions doped zinc bismuth borate glasses. *J Alloys Compd* 509:7625–7631
- [39] Judd BR (1962) Optical absorption intensities of rare-earth ions. *Phys Rev* 127:750–761
- [40] Ofelt GS (1962) Intensities of crystal spectra of rare-earth ions. *J Chem Phys* 37:511–520
- [41] Manzani D, Paboeuf D, Ribeiro SJL, Goldner P, Bretenaker F (2013) Orange emission in Pr^{3+} -doped fluorindate glasses. *Opt Mater* 35:383–386
- [42] Goldner P, Auzel F (1996) Application of standard and modified Judd-Ofelt theories to a praseodymium doped fluorozirconate glass. *J Appl Phys* 79:7972
- [43] Srinivasa Rao L, Reddy MS, Reddy MVR, Veeraiah N (2008) Spectroscopic features of Pr^{3+} , Nd^{3+} , Sm^{3+} and Er^{3+} ions in $\text{Li}_2\text{O}-\text{MO}$ (Nb_2O_5 , MoO_3 and WO_3)- B_2O_3 glass systems. *Physica B* 403:2542–2556
- [44] Srivastava P, Rai SB, Rai DK (2004) Effect of lead oxide on optical properties of Pr^{3+} doped some borate based glasses. *J Alloys Compd* 368:1–7
- [45] Metha V, Aka G, Dawar AL, Mansingh A (1999) Optical properties and spectroscopic parameters of Nd^{3+} doped phosphate and borate glasses. *Opt Mater* 12:53–63
- [46] Quimby RS, Miniscalco WJ (1994) Modified Judd-Ofelt technique and application to optical transitions in Pr^{3+} doped glass. *J Appl Phys* 75:613
- [47] Seeber W, Downing EA, Hesselink L, Fejer MM, Ehrt D (1995) Pr^{3+} -doped fluoride glasses. *J Non-Cryst Solids* 189:218–226

- [48] Henry ND, Adam JL, Jacquier B, Linares C (1996) Photoluminescence of new fluorophosphate glasses containing a high concentration of terbium (III) ions. *Opt Mater* 5:197–207
- [49] Sourkova P, Frumarova B, Fruma M, Nemeč P, Kincl M, Nazabal V, Moizan V, Doualan JL, Moncorge R (2009) Spectroscopy of infrared transitions of Pr^{3+} ions in Ga–Ge–Sb–Se glasses. *J Lumin* 129:1148–1153
- [50] Klimesz B, Dominiak-Dzik G, Solarz P, Żelechower M, Romanowski WR (2005) Optical study of GeO_2 – PbO – PbF_2 oxyfluoride glass singly doped with Pr^{3+} , Nd^{3+} , Sm^{3+} and Eu^{3+} . *J Alloys Compd* 403:76–85
- [51] Voda M, Balda R, Saleh MA, Ocariz ISD, Cano M, Lobera G, Macho E, Fernández J (2001) Optical properties of Pr -doped lithium tetraborate glasses. *J Alloys Compd* 12:250–254
- [52] Mitra S, Jana S (2015) Intense orange emission in Pr^{3+} doped lead phosphate glass. *J Phys Chem Solids* 85:245–253
- [53] Man SQ, Pun EYB, Chung PS (1999) Tellurite glasses for 1.3 μm optical amplifiers. *Opt Commun* 168:369–373
- [54] Jamalaiah BC, Suresh Kumar J, Babu AM, Rama Moorthy L, Jang K, Lee HS, Jayasimhadri M, Jeong JH, Choi H (2009) Optical absorption, fluorescence and decay properties of Pr^{3+} -doped PbO – H_3BO_3 – TiO_2 – AlF_3 glasses. *J Lumin* 129:1023–1028
- [55] Dzika GD, Romanowski WR, Pisarska J, Pisarski WA (2007) Spectral properties and dynamics of luminescent states of Pr^{3+} and Tm^{3+} in lead borate glasses modified by PbF_2 . *J Lumin* 122–123:62–65
- [56] Vijaya Kumar MV, Rama Gopal K, Reddy RR, Reddy GVL, Hussain NS, Jamalaiah BC (2013) Application of modified Judd-Ofelt theory and the evaluation of radiative properties of Pr^{3+} -doped lead telluroborate glasses for laser applications. *J Non-Cryst Solids* 364:20–27